



Polymer composite containing nano magnesium oxide filler and lithiumtriflate salt: An efficient polymer electrolyte for lithium ion batteries application

Emad M. Masoud^{a,b,*}, A.-A. El-Bellihi^a, Wafaa A. Bayoumy^a, Eman A. Mohamed^a

^a Chemistry Department, Faculty of Science, Benha University, 13518 Benha, Egypt

^b Textile Engineering Department, Chemistry and Science, College of Textiles, North Carolina State University, Raleigh, NC 27695-8301, USA

ARTICLE INFO

Article history:

Received 7 January 2018

Received in revised form 15 March 2018

Accepted 20 March 2018

Available online 22 March 2018

Keywords:

Polymer nano composites electrolytes

Electrical properties

Thermal stability

Electrochemical stability

Lithium ion batteries

ABSTRACT

Polymer (PVdF-CO-HFP) composites containing nano MgO filler and lithiumtriflate salt were prepared using a solution cast technique. All samples were characterized using different techniques such as X-ray diffraction (XRD), thermal analysis (TG, DSC), Fourier transform infra-red spectroscopy (FT-IR) and scanning electron microscopy (SEM). Structural investigation of all samples were conducted in a well - sequence; firstly, in presence of nano filler, and secondly in presence of LTF salt to study the structural changes (crystallinity), and their effects on melting, morphology and thermal stability behavior. In presence of definite filler and salt concentrations, the basic polymer matrix exhibited suitable structure, followed by good conduction properties. A sample containing 6 wt% MgO and 25 wt% LTF showed AC-ionic conductivity value of about $8.78 \times 10^{-5} \text{ ohm}^{-1} \cdot \text{cm}^{-1}$ at room temperature. The same sample exhibited good thermal stability behavior ($T_d = 402.99^\circ\text{C}$). To further investigate the stability of this sample, electrochemical and mechanical stability properties were also studied.

© 2018 Elsevier B.V. All rights reserved.

1. Introduction

The research and development of polymer electrolyte based batteries with high specific energy, good reliability and safety has been an active area for the past three decades [1–3]. Advances in microelectronic industry, especially mobile phones and portable computers, have created a demand for new and improved power sources. Presently, world-wide efforts are directed towards the development of advanced battery technologies based on lithium negative electrodes (anode).

To date, the rechargeable lithium ion battery has been one of the best choices in view of specific capacity and cyclic stability [4]. However, the electrolytes which are used in the rechargeable lithium ion battery still need improvement especially in terms of ionic conductivity at room temperature, thermal stability and mechanical stability [5]. To accomplish these requirements, extensive research has been conducted on several polymer hosts [6–13]. Among the various polymers, the PVdF-CO-HFP based electrolyte has received much attention due to its unique properties i.e. the host polymer possesses both amorphous and crystalline phases in which the crystalline VdF phase acts as a mechanical stiffer

and the amorphous HFP phase helps in improving the ionic conductivity [14,15]. The positive effect of various ceramic particles, like SiO_2 , TiO_2 , Al_2O_3 , etc., on the conductivities and electrochemical stability of polymer electrolytes is also well documented in the literature [16–18]. The addition of the fillers with Lewis acids surface groups usually leads to reduction in ion pairing and therefore to an increase in the conductivity. On the other hand, stabilization of the interphase and lowering of the overall resistance of lithium electrodes was observed when using surface modified inorganic fillers as additives [19–21].

Many researchers present encouraging results for P (VdF-HFP)-based polymer electrolytes with different types of dopant salts, such as lithium fluoroalkyl phosphate [22], lithium perchlorate [23] and lithium bis(trifluoromethanesulfonyl)imide [24]. Lithium trifluoromethanesulfonate salt, LTFMS, is one of the most common lithium salts used in polymer electrolyte research. As a continuation of our previous studies on polymer electrolytes materials, we try to prepare a novel polymer composite delivering a high ionic conductivity and good thermally stable behavior, to be used as an efficient polymer electrolyte for the lithium ion batteries applications. On this way and in our present work, we try to use nano filler with a suitable concentration achieving the two main properties of the electrolyte; ionic conductivity and thermal stability. Nano magnesium oxide (MgO) filler; one of the fillers that has not been used enough to enhance the polymer electrolyte performance, especially the thermal stability behavior. In this research paper, a gel composite of PVdF-CO-HFP, Ethylene carbonate (EC) and

* Corresponding author at: Chemistry Department, Faculty of Science, Benha University, 13518 Benha, Egypt.

E-mail addresses: emad.youssef@fsc.bu.edu.eg, emad_masoud1981@yahoo.com, (E.M. Masoud).

URL: <http://www.bu.edu.eg/staff/emadyoussef7>

Diethyl carbonate (DEC) containing lithium trifluoromethanesulfonate as a salt and nano magnesium oxide (MgO) as filler will be studied

and investigated in different concentrations of both salt and filler to achieve the required electrolyte properties of conductivity and stability.

2. Experimental

2.1. Preparation of nano magnesium oxide filler

Nano magnesium oxide filler was prepared using the solution combustion process [25]. Briefly, appropriate amounts of $\text{Mg}(\text{NO}_3)_2$ and urea (used as a fuel) were dissolved in distilled water. Following, the above solution was heated to dryness at 100 °C and then the dried mass was calcined at around 450 °C for 5 h to get MgO filler.

2.2. Preparation of polymer nano composites

The polymer nano composites were prepared using a simple solution casting technique. PVdF-CO-HFP was first dissolved in di-methyl formamide (DMF) under heating (40 °C). Following, plasticizers (EC: DEC, 1:1 in volume) were added to the polymer viscous solution. After that, different MgO filler amounts were added according to the following concentration formula:

$$[[33-x(\text{PVdF-CO-HFP}) + 67(\text{EC-DEC}) + x(\text{MgO})], x = 0, 2, 4, 6 \text{ wt}\%]$$

The slurry was continuously stirred for 24 h to avoid the filler aggregation and to get the fine mixing. The obtained homogenous viscous slurry was then poured into the Petri dish. The solvent was allowed to evaporate slowly from the composite at room temperature and then all samples were dried at 60 °C for 3 h to get nano composites membranes.

2.3. Preparation of polymer nano composites electrolytes

The polymer nano composites electrolytes were prepared using the same method and according to the following concentration formula:

$$[[\text{PVdF-CO-HFP} + (\text{EC-DEC}) + (\text{MgO})]_{100-x} + x(\text{LiCF}_3\text{SO}_3), x = 0, 5, 15, 25 \text{ wt}\%]$$

Similarly to the first preparation, the stirring, pouring, and solvent evaporation processes were performed to get nano composites electrolytes membranes having a thickness between 330 and 350 μm .

Additionally, and to easy hereafter mention all investigated different samples, all samples were denoted as following:

Samples containing PVdF-CO-HFP, EC, DEC and nano MgO filler were denoted as MC1, MC2 and MC3; for nano MgO filler concentrations: 2, 4 and 6 wt%, respectively. In contrast, samples containing PVdF-CO-HFP, EC, DEC, optimized nano MgO filler concentration and lithiumtriflate were denoted as MCE1, MCE2 and MCE3; for lithiumtriflate salt concentrations: 5, 15 and 25 wt%, respectively. Also, lithiumtriflate salt was denoted as LTF.

2.4. Characterization of samples

X-ray diffraction analysis was performed on a Diano (made by Diano Corporation, U.S.A.) with Cu-filtered $\text{CuK}\alpha$ radiation ($\lambda = 1.5418 \text{ \AA}$) energized at 45 kV, and 10 mA. The samples were measured at room temperature in the range from $2\theta = 10$ to 70° . Differential scanning calorimetry (DSC, in a temperature range of 298–473 K) and thermal gravimetric analysis (TG, in a temperature range of 298–873 K) were performed in air atmosphere with a constant heating rate of 10 °C/min using Shimadzu DSC-60H. The Fourier transform infrared spectra of the samples were recorded in the range of 650–4000 cm^{-1} using a Bruker - FT-IR. Scanning electron microscopy was carried out with JOEL scanning electron microscope (JSM-35CF). The thickness of each sample was measured using a micrometer screw gauge. Electrical properties were studied in a temperature range from 298 to 423 K and a frequency one from 100 Hz to 1 MHz. Also, these properties were estimated with the help of stainless steel blocking electrodes using a programmable automatic LCR bridge (Model RM 6306 Phillips Bridge).

The electrochemical stability of optimized composite electrolyte of high ionic conductivity was evaluated using a stainless steel (SS) as working and counter electrode, by linear sweep voltammetry at room temperature using an EG&G Electrochemical analyzer (Model-6310) in the scan rate of 1 mV/s. The mechanical properties (stress-strain characteristic) were studied at room temperature using Bruker - Digital force gauge (1000 N). The sample was cast in a dimension of 60 mm \times 20 mm. The thickness of cast sample is 2 mm.

3. Results and discussion

3.1. Effect of MgO filler concentration on PVdF-co-HFP

3.1.1. X-ray diffraction analysis

X-ray diffraction patterns of MgO, PVdF-co-HFP, MC1, MC2 and MC3 are displayed in Fig. 1. The pattern of MgO filler revealed a single phase cubic structure. The particle size of MgO was calculated by means of the well-known Debye Scherer's formula [26]. Thus, the mean crystallite size of MgO was found to be 40 nm. In contrast, the XRD pattern of the PVdF-CO-HFP polymer confirmed its semi crystalline nature [27]. Furthermore, as obviously observed, the nano MgO filler presence in MC1, MC2 and MC3 samples was confirmed by the weak peaks.

Moreover, the filler showed an effect on the semi crystalline nature of PVdF-CO-HFP, as weak and sharp peaks were observed. This means that there is an interaction between the filler and the polymer, and also means that the three samples have different crystalline structure percent in presence of the different nano MgO filler concentrations. Also, from Fig. 1, one can conclude that the MC3 sample has the lowest crystalline structure percent compared to MC2 and MC3 ones, as more weak peaks observed.

3.1.2. Differential scanning calorimetry (DSC) analysis

DSC thermograms of PVdF-CO-HFP, MC1, MC2 and MC3 are shown in Fig. 2. Obviously, the peak observed at a temperature range between 160.61 and 163.34 °C for all investigated samples was mainly due to the

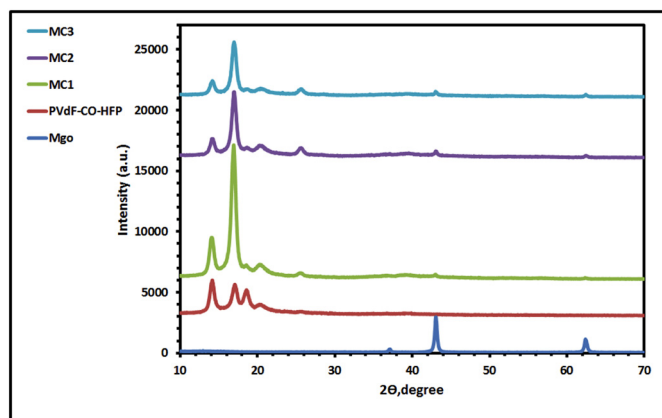


Fig. 1. X-ray diffraction patterns of MgO, PVdF-CO-HFP, MC1, MC2 and MC3.

melting temperature (T_m). All values of melting temperatures were exactly determined and tabulated, Table 1. As we can see, the nano MgO filler samples showed higher T_m than that of PVdF-co-HFP; and MC3 sample showed the lowest one value compared to MC1 and MC2. These melting temperatures values come in a good matching with what observed above. As mentioned in X-ray diffraction analysis, the MC3 sample has the weakest crystalline peaks; and here DSC one confirmed that it has the lowest melting temperature (T_m , 160.92 °C). This shows that the sample of the lowest crystalline structure has the lowest melting temperature (T_m). Also, to practically confirm this point, all values of crystallinity relative percentage (X_c) were calculated using the equation [28]:

$$X_c = \Delta H_c / \Delta H_p \quad (1)$$

where ΔH_p equals to 104.7 J/g which is the heat enthalpy of 100% crystalline PVdF [29], and ΔH_c is the heat enthalpy of PVdF-co-HFP, MC1, MC2 and MC3. All values were tabulated, Table 1. As shown, crystallinity

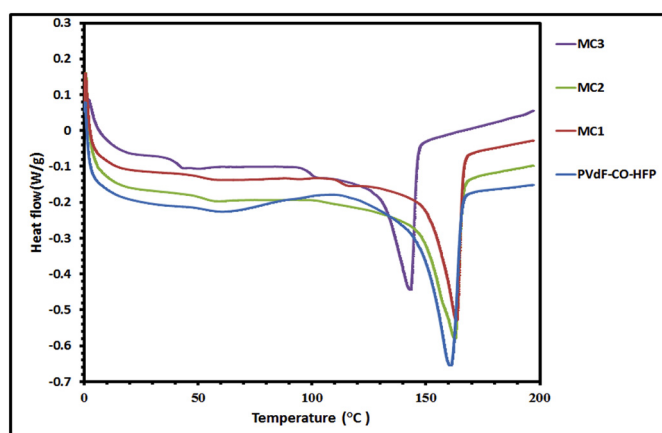


Fig. 2. Thermal analysis (DSC) patterns of PVdF-CO-HFP, MC1, MC2 and MC3.

Table 1
Values of melting temperature (T_m), heat enthalpy of melting (ΔH_m) and crystallinity percent (X_c) of PVdF - CO - HFP, MC1, MC2 and MC3.

Sample	T_m , °C	ΔH_m , J/g	X_c , %
PVdF - CO - HFP	160.61	37.81	36.11
MC1	163.34	27.59	26.35
MC2	161.81	30.14	28.79
MC3	160.92	20.74	19.81

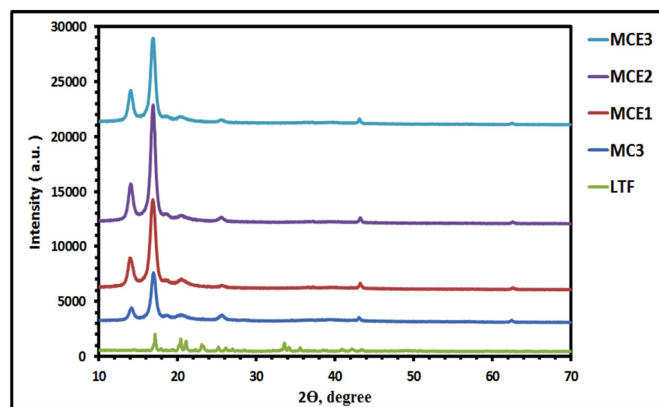


Fig. 3. X-ray diffraction patterns of LTF, MC3, MCE1, MCE2 and MCE3.

relative percentage confirmed all mentioned above. The MC3 sample showed the lowest value (19.81%) compared to MC1 (26.35%) and MC2 (28.79%).

3.2. Effect of LTF concentration on MC3

3.2.1. X-ray diffraction analysis

Fig. 3 shows X-ray diffraction patterns of LTF, MC3, MCE1, MCE2 and MCE3. The figure showed the good dissolution behavior of PVdF-CO-HFP matrix in presence of nano MgO filler, as LTF peaks completely disappeared in all MCE1, MCE2 and MCE3 samples. This means that all LTF concentrations were completely dissolved in MC3 sample. More notably, LTF samples (MCE1 and MCE3) showed lower intensive crystalline peaks than that of MCE2. This also can confirm the different interactions presence between LTF and MC3 sample.

3.2.2. Differential scanning calorimetry (DSC) analysis

As shown in Fig. 4, thermograms of MC3, MCE1, MCE2 and MCE3, showed that LTF samples have lower melting temperature (T_m) values than that of MC3, as observed by peak decrease shifting. Moreover, the MCE3 sample showed the lowest melting temperature value compared to MCE1 and MCE2 samples. This also supports our previous observation of X-ray diffraction analysis, as the same sample has low intensive crystalline peak. All melting temperatures (T_m) values were also exactly determined and tabulated, Table 2.

Also, to investigate and confirm the crystallinity structure of LTF samples, all relative crystalline percentage (X_c , %) values were calculated using Eq. (1). All values were tabulated, Table 2. The table showed that the MCE3 sample has the lowest value (24.97%) compared to MCE1

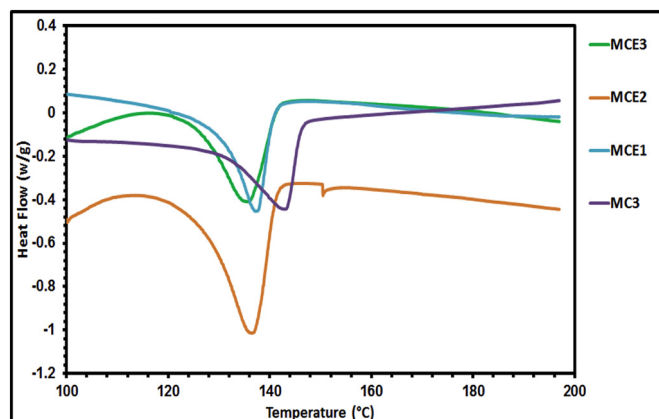


Fig. 4. Thermal analysis (DSC) patterns of MC3, MCE1, MCE2 and MCE3.

Table 2

Values of melting temperature (T_m), heat enthalpy of melting (ΔH_m), crystallinity percent (X_c), decomposition temperature (T_d) and AC-ionic conductivity (σ_{AC}) of PVdF - CO - HFP, MC3, MCE1, MCE2 and MCE3.

Sample	T_m , °C	ΔH_m , J/g	X_c , %	T_d , °C	σ_{AC} ($\text{ohm}^{-1} \cdot \text{cm}^{-1}$) at 303 K
PVdF - CO - HFP	160.61	37.81	36.11	431.92	1.5×10^{-10}
MC3	160.92	20.74	19.81	454.68	1.95×10^{-7}
MCE1	161.63	29.41	28.09	386.24	2.14×10^{-5}
MCE2	160.73	40.51	38.69	396.49	5.27×10^{-5}
MCE3	159.97	26.14	24.97	402.99	8.78×10^{-5}

(28.09%) and MCE2 (38.69%). Here, above discussion can also be confirmed, as low intensive crystalline peak, lowest melting temperature (159.97 °C) sample has the lowest crystalline structure (24.97%).

3.3. Thermal stability behavior

As membrane thermal stability is one of the most important properties of polymer nano composite electrolyte application, thermal gravimetric analysis, TG, was studied to investigate the effect of both nano MgO filler and LTF on PVdF-CO-HFP matrix. Fig. 5 shows thermal patterns of PVdF-CO-HFP, MC3, MCE1, MCE2 and MCE3. As we can see, all samples showed almost stable weight against temperature, but till different certain temperatures. In general, the slightly weight decrease up to 400 °C may be attributed to both of the removal of moisture and/or the absorbance of water by the sample during the loading and melting. Following, the sharp weight decrease of all samples can be attributed to the degradation of the side chains of the polymer. Additionally, the different remaining weight percentage of all samples could be due to the presence of nano MgO filler or due to the presence of —CF based back bones of the PVdF-CO-HFP polymer [30]. All degradation temperatures (T_d) of all investigated samples were exactly determined and tabulated, Table 2. From table, we can conclude that the MC3 sample showed higher decomposition temperature ($T_d = 454.68$ °C) than that of PVdF-CO-HFP ($T_d = 431.92$ °C), and this also can confirm the nano filler interactions with the polymer matrix. On the other hand, LTF samples showed the following decomposition temperature (T_d) order: [MCE3, $T_d = 402.99$ °C > MCE2, $T_d = 396.49$ °C > MCE1, $T_d = 386.24$ °C]. So we can conclude that the LTF sample (MCE3) has the highest thermal stability behavior compared to the other ones. This sample can introduce also the lowest crystalline structure in addition to the melting temperature, the features of a good polymer nano composite electrolyte.

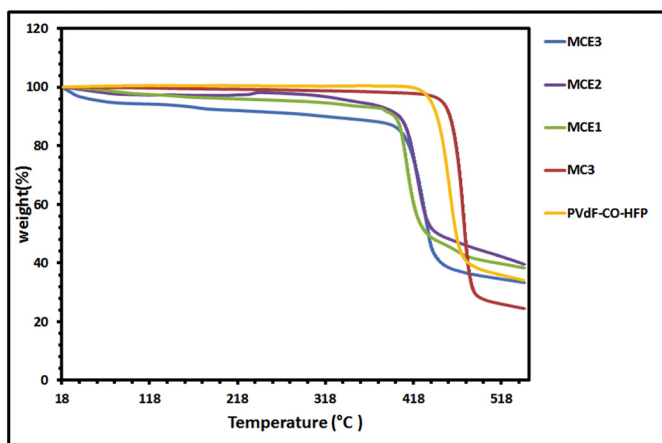


Fig. 5. Thermal analysis (TG) patterns of PVdF-CO-HFP, MC3, MCE1, MCE2 and MCE3.

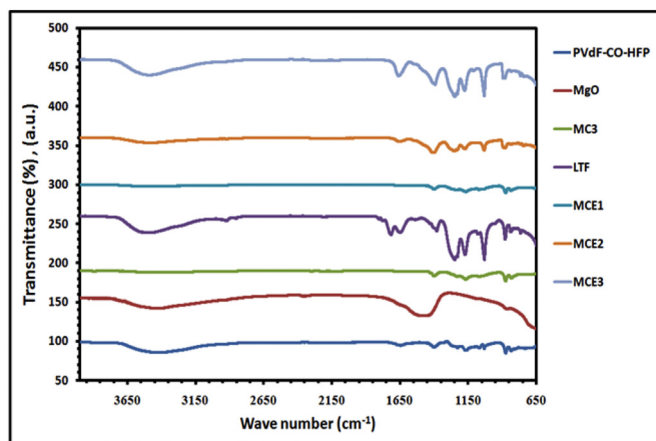


Fig. 6. FT-IR spectra of PVdF-CO-HFP, MgO, MC3, LTF, MCE1, MCE2 and MCE3.

3.4. FT-IR analysis

Fig. 6 shows FT-IR spectra of PVdF-CO-HFP, MgO, MC3, LTF, MCE1, MCE2 and MCE3. The basic characteristic bands of PVdF-CO-HFP [30] are shown in Table 3. To investigate and also confirm the interactions that can take place between nano MgO filler and polymer matrix, PVdF-CO-HFP, a comparison between the wave number values of the basic polymer matrix and basic polymer matrix containing nano MgO filler (MC3) was established, Table 3. As seen, there is an observed decrease/increase shifting in wave number values of MC3 sample, confirming the interactions presence between the two components. Likewise, an observed decrease/increase shifting between MC3 and LTF samples (MCE1, MCE2 and MCE3) was also observed, Table 3, and also confirmed the interactions presence between LTF and polymer matrix (MC3).

3.5. Scanning electron microscope (SEM)

As well known, the basic polymer matrix of PVdF-CO-HFP has a porous structure. So an investigation of the morphology porous nature in presence of nano MgO filler and LTF was performed using FE - scanning electron microscope, FE-SEM, Fig. 7(A, B). Fig. 7A showed the porous structure of the basic polymer matrix, PVdF-CO-HFP. In contrast, Fig. 7B revealed a non-porous structure, reflecting the good role of nano filler and salt in filling the polymer matrix pores with a homogeneous nature. This filling process attributed the thermal decomposition temperature increase of MC3 compared to the basic polymer matrix, PVdF-CO-HFP, Table 2.

3.6. Electrical conductivity properties

The temperature dependence of AC - electrical conductivity of PVdF-CO-HFP, MC3, MCE1, MCE2 and MCE3 was investigated in a temperature range of 303–423 K and at a frequency of 100 Hz, and illustrated in Fig. 8. In general, the figure shows that the AC-conductivity of all investigated samples increases with temperature increase. As the

Table 3

FT-IR spectral basic bands assignment of PVdF - CO - HFP, MC3, MCE1, MCE2 and MCE3.

Wave number (cm^{-1})	PVdF - CO - HFP	MC3	MCE1	MCE2	MCE3
763	Crystalline phase VdF unit of PVDF-CO-HFP	751	758	742	765
1200	—CF ₂ group of PVdF-CO-HFP	1209	1213	1214	1199
1390	CF ₂ - deformation of PVdF-CO-HFP	1399	1370	1394	1383

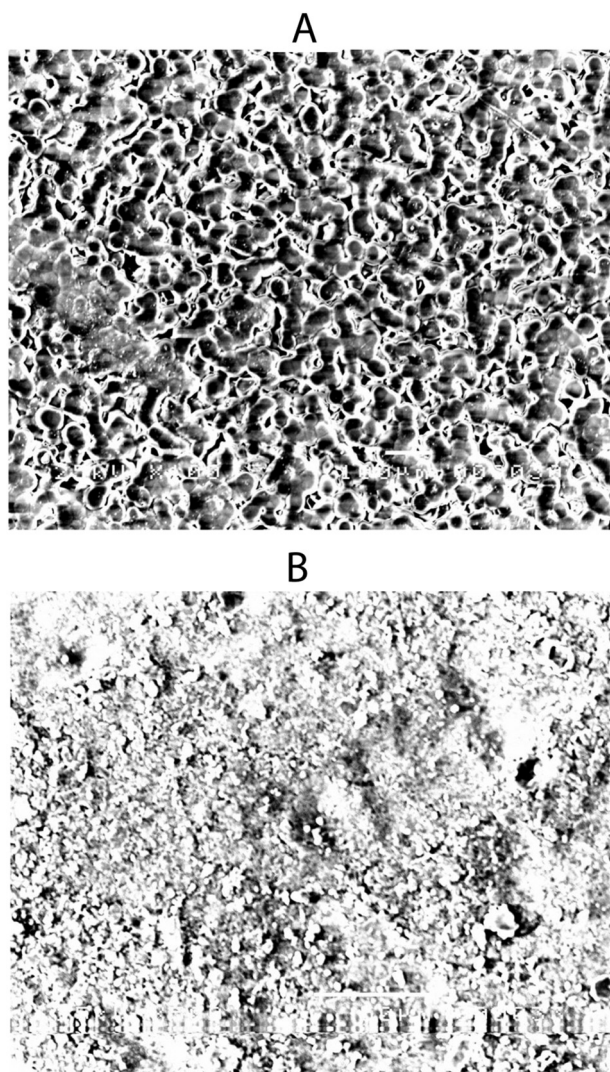


Fig. 7. FE-SEM photographs of A: PVdF - CO - HFP and B: MCE3.

conductivity–temperature data follow Arrhenius behavior, the mechanism of ion transport is deduced to be similar to that in ionic crystals, where ions jump into neighboring vacant sites and thus increase the ionic conductivity to a higher value. The motion of ions in polymer electrolytes is a liquid-like mechanism, by which the movement of ions

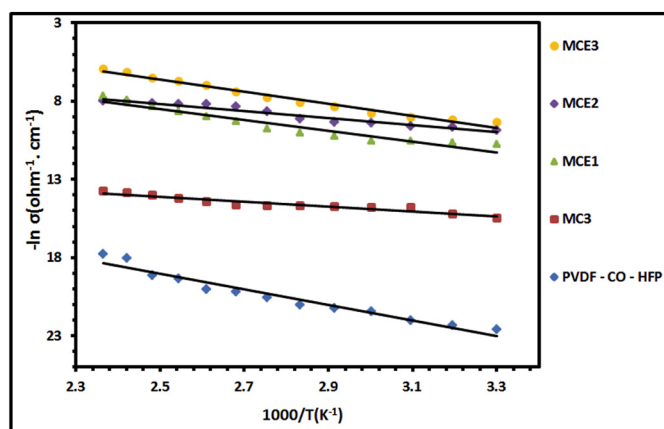


Fig. 8. Temperature dependence of AC-conductivity for PVdF-CO-HFP, MC3, MCE1, MCE2 and MCE3 at a frequency of 100 Hz.

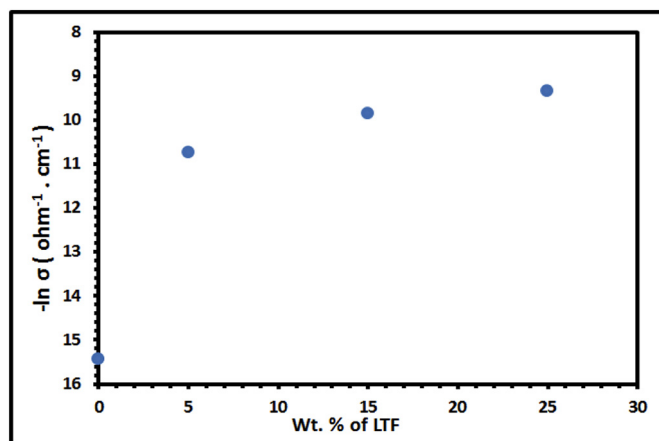


Fig. 9. AC-conductivity values versus LTF concentration (wt.%) for MC3, MCE1, MCE2 and MCE3 at room temperature and a frequency of 100 Hz.

through the polymer matrix is assisted by the large amplitude of the polymer segmental motion. Thus, greater segmental motion at higher temperatures either permits the ions to hop from one site to another or provides a pathway for ions to move with faster ionic conduction. Additionally, the figure showed the positive effect of nano MgO filler on increasing the AC-conductivity of the basic polymer matrix of PVdF-CO-HFP, where MC3 sample showed higher AC-conductivity values than that of PVdF-CO-HFP. The filler can play two important roles in increasing the conductivity; the first is its ability to decrease the crystallinity of the basic polymer matrix as previously confirmed by DSC analysis, and the second is as suggested by Coce et al. [31]; the filler can provide special conducting pathways at the filler surface region through Lewis acid – base interactions among different species in the polymer matrix. At the same time, all LTF samples showed higher AC-conductivity values compared to that of MC3, reflecting the positive effect of LTF salt on increasing the AC-conductivity of MC3 sample. All room temperature AC-conductivity values are tabulated, Table 2. Also, the effect of LTF salt addition on MC3 sample at room temperature and a frequency of 100 Hz was shown in Fig. 9. The figure revealed the continuous increase of AC-conductivity value upon LTF salt concentration increase. The AC-conductivity values have the following order: $[\sigma_{AC}(\text{MCE3}, 8.78 \times 10^{-5} \text{ ohm}^{-1} \cdot \text{cm}^{-1}) > \sigma_{AC}(\text{MCE2}, 5.27 \times 10^{-5} \text{ ohm}^{-1} \cdot \text{cm}^{-1}) > \sigma_{AC}(\text{MCE1}, 2.14 \times 10^{-5} \text{ ohm}^{-1} \cdot \text{cm}^{-1}) > \sigma_{AC}(\text{MC3}, 1.95 \times 10^{-7} \text{ ohm}^{-1} \cdot \text{cm}^{-1})]$. Here, it is worthwhile to mention that the sample having the lowest crystalline structure, lowest melting temperature and highest thermal stability is the same having

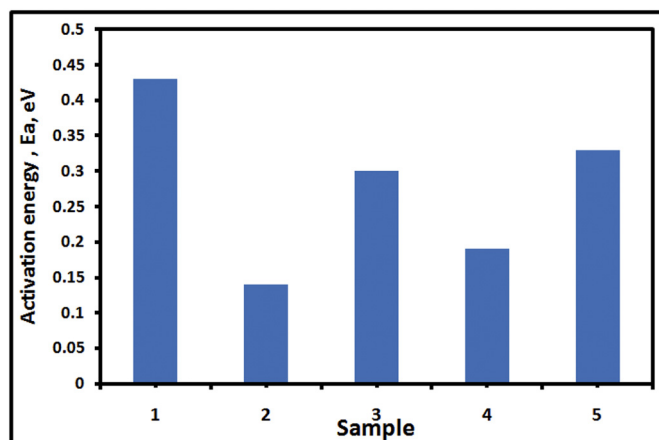


Fig. 10. Activation energy values of 1: PVdF - CO - HFP, 2: MC3, 3: MCE1, 4: MCE2 and 5: MCE3.

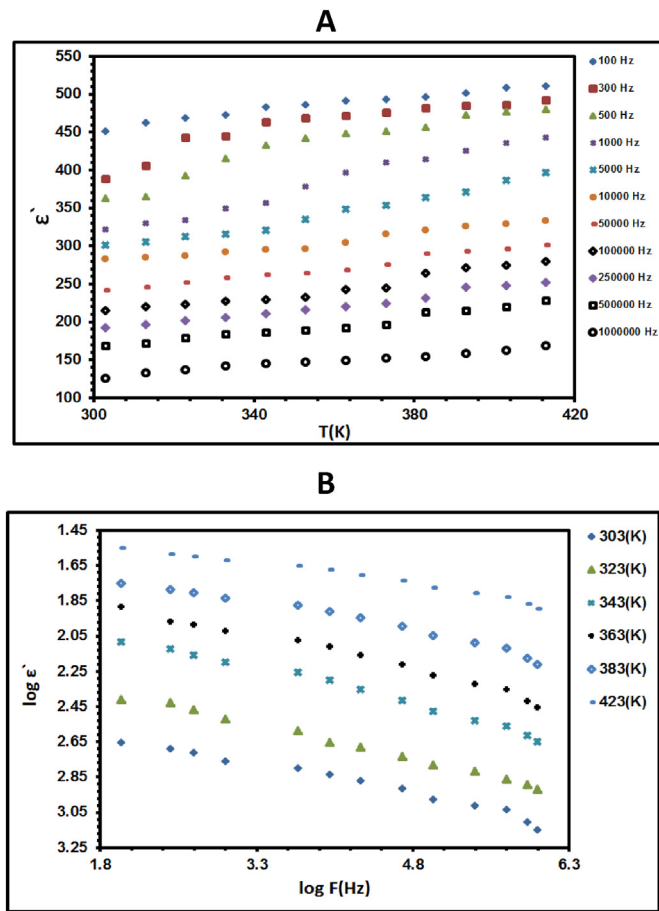


Fig. 11. Dielectric constant versus A: temperature; at different frequencies and B: frequency; at different temperatures for MCE3 sample.

the highest AC-conductivity value at room temperature. This feature confirms our previous structural properties investigation results of this sample.

Furthermore, as curves appear linear, so the apparent activation energies (E_a) are obtained using the Arrhenius model $\sigma = \sigma_0 \exp(-E_a/RT)$, where R , T , σ and σ_0 are gas constant, temperature, the AC-conductivity and the pre-exponential factor, respectively. According to this equation, the activation energies can be calculated from the slope of straight line. All activation energy values were shown in Fig. 10. The activation energies (E_a) values come as in the following order: [E_a (MC3) < E_a (MCE2) < E_a (MCE1) < E_a (MCE3) < E_a (PVdF-CO-HFP)].

As a conclusion and from all above investigations, the MCE3 sample is the best one delivering good conductivity value at room temperature. So more studies will be conducted hereafter to investigate this sample, and to confirm its ability to be an efficient polymer electrolyte within lithium ion batteries.

3.7. Dielectric constant

Temperature and frequency dependence of dielectric constant at different frequencies (100 Hz to 1 MHz) and temperatures (303 to 423 K), respectively of optimized MCE3 sample was also studied, Fig. 11(A, B). Firstly, Fig. 11A showed an increase behavior of dielectric constant with temperature at different frequencies. It is observed that this increase behavior can be divided into two ranges; weakly dependent one (303–353 K), and other strongly one (363–413 K). Generally, the increase behavior of dielectric constant with temperature can be attributed to the viscosity decrease [32] of the polymer matrix, and dissolving of crystalline or semi-crystalline phases in the amorphous phase [33]. Secondly, Fig. 11B represented a decrease behavior of

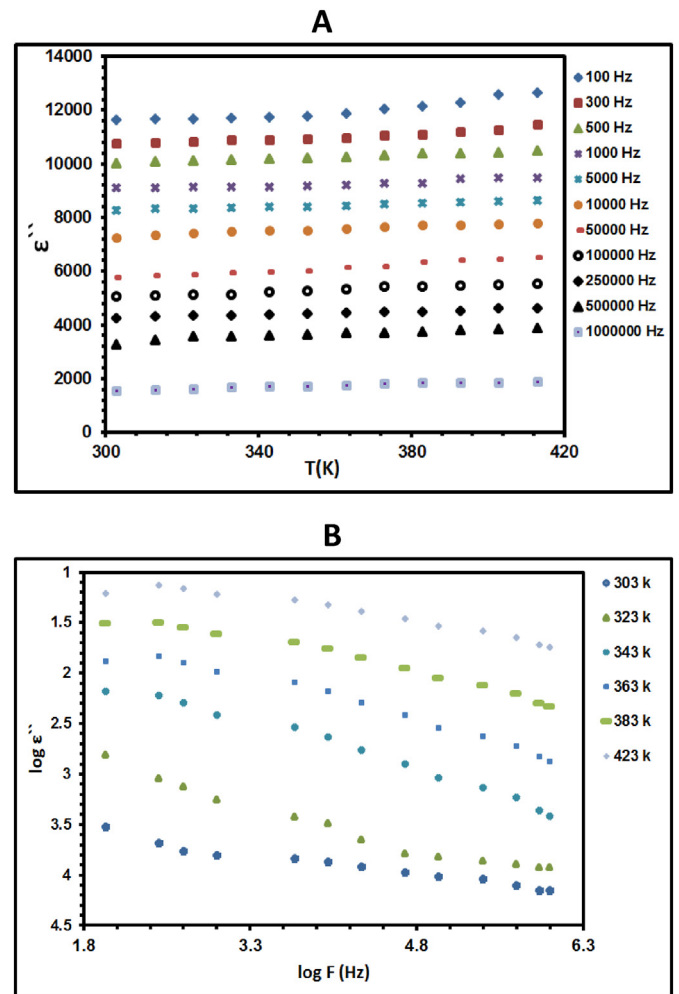


Fig. 12. Dielectric loss versus A: temperature; at different frequencies and B: frequency; at different temperatures for MCE3 sample.

dielectric constant with frequency at different temperatures. This decrease behavior can be attributed to the contribution of charge accumulation at the interface and leads to a net polarization of the ionic medium results in the formation of space charge region at electrode-electrolyte interface [34]. The MCE3 sample exhibited a value of dielectric constant (ϵ') equals 450 at room temperature (303 K) and 100 Hz.

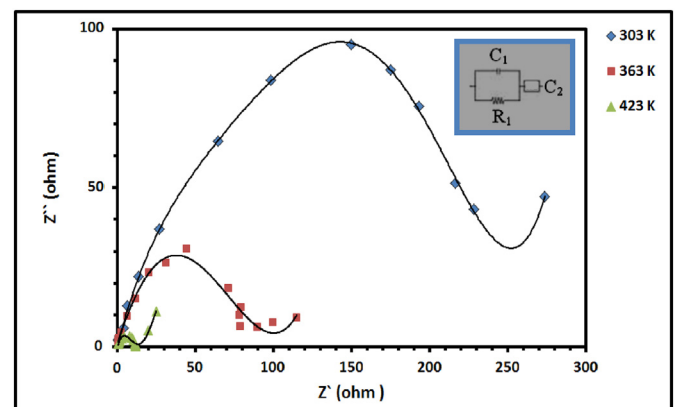


Fig. 13. Complex impedance spectra for MCE3 sample at different temperatures.

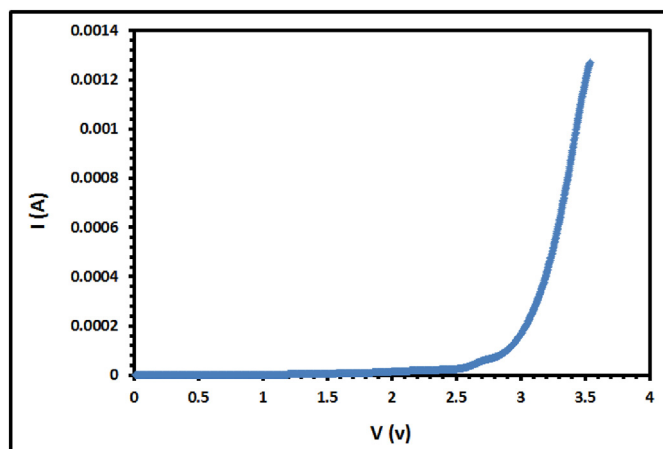


Fig. 14. I-V curve for MCE3 sample at room temperature.

3.8. Dielectric loss

Temperature and frequency dependence of dielectric loss at different frequencies (100 Hz to 1 MHz) and temperatures (303 to 423 K), respectively of optimized MCE3 sample was also studied, Fig. 12(A, B). Firstly, Fig. 12A showed an increase behavior of dielectric loss with temperature at different frequencies. This increase behavior is due to the relaxation of the dipole molecules in co-operation with the resulting drop in the relaxation time, this in turns exerts a double effect on the dielectric loss, on one hand, the friction between the dipoles will be increased and then the increase in energy dissipation. Secondly, Fig. 12B showed a logic decrease behavior of dielectric loss with frequency at different temperatures. The MCE3 sample exhibited a value of dielectric loss (ϵ'') equals 11,750 at room temperature (303 K) and 100 Hz.

3.9. Complex impedance

Fig. 13 shows a complex impedance of MCE3 sample at three different temperatures (303, 363, and 423 K). The figure exhibited a spectrum consists of a semi-circle and an inclined straight line. As obviously shown, the diameter and height of semi-circles decreases upon temperature increasing, reflecting the impedance decrease with temperature increase. The semicircle is due to the conduction process and the

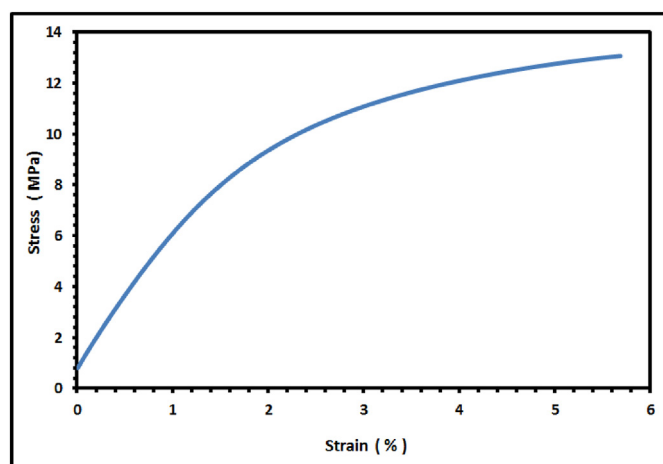


Fig. 15. Stress - strain curve for MCE3 sample at room temperature.

linear region is due to the effect of the blocking electrode [35–39] that results in a charge polarization in the bulk of the polymer. All bulk ionic conductivity values were calculated at different temperatures and exhibited the following order: [$(\sigma_b = 7.02 \times 10^{-5} \text{ ohm}^{-1} \cdot \text{cm}^{-1}$ at 303 K) < $(\sigma_b = 2.00 \times 10^{-4} \text{ ohm}^{-1} \cdot \text{cm}^{-1}$ at 363 K) < $(\sigma_b = 1.23 \times 10^{-3} \text{ ohm}^{-1} \cdot \text{cm}^{-1}$ at 423 K)]. The equivalent circuit was also determined from the spectrum and shown in Fig. 13. Where R1 is the bulk resistance of the electrolyte, C₁ is the bulk capacity of the electrolyte and C₂ is a capacity of bulk electrode – electrolyte interface.

3.10. Electrochemical stability of MCE3

Fig. 14 shows the I-V characteristic curve. The onset voltage for anodic current is determined at around 3 V which is assumed to be the decomposition voltage of the optimized sample (MCE3).

3.11. Mechanical properties of MCE3

The stress – strain curve of the optimized sample (MCE3) was also investigated, Fig. 15. The figure showed yield strength of about 1 MPa with an elongation –at- break of 5.7%. Also, the energy per unit volume i.e. toughness is 0.12 J.

4. Conclusions

Nano magnesium oxide filler was prepared using the solution combustion process. Different polymer nano composites were prepared using solution cast technique. Structural investigation of all samples were conducted in a well – sequence; firstly, in presence of nano filler, and secondly in presence of LTF salt to study the structural changes (crystallinity) and their effects on melting, morphology and thermal stability behavior. Different techniques such as X-ray diffraction, FT-IR, SEM, TG and DSC were used to study these changes. In brief, the addition of nano filler and LTF salt exhibited an obvious effect on the basic polymer matrix, PvdF-CO-HFP. With a concentration of 6 wt% MgO and 25 wt% LTF, the optimized sample (MCE3) showed low crystalline structure ($X_c = 24.97\%$) and melting temperature (159.97°C) with a good thermal stability behavior ($T_d = 402.99^\circ\text{C}$). Electrical conductivity properties of this sample were completely studied. The sample showed values of AC-ionic conductivity, dielectric constant, dielectric loss and bulk ionic conductivity equal $8.78 \times 10^{-5} \text{ ohm}^{-1} \cdot \text{cm}^{-1}$, 450, 11,750 and $7.02 \times 10^{-5} \text{ ohm}^{-1} \cdot \text{cm}^{-1}$ at room temperature and 100 Hz, respectively. Additionally, the sample exhibited good electrochemical (decomposition voltage = 3 V) and mechanical (an elongation –at-break of 5.7%) stability. At last, we can conclude that using nano MgO filler and LTF salt in definite concentrations with the basic polymer matrix formed a suitable matrix structure for lithium ions motion, making this polymer nano composite electrolyte sample a promised thermally stable electrolyte for lithium – ion batteries application.

Acknowledgment

The first and corresponding author (Emad M. Masoud) of this manuscript would like to thank Science and Technology Development Fund (STDF), Egypt, (<http://www.stdf.org.eg/index.php/en/>) for the financial support of this scientific research work through Short-Term Fellowship (STF-23173) project. Also, my sincere thanks to Prof. Dr. Xiangwu Zhang (College of textiles, North Carolina State University, USA) for his acceptance to perform a part of this work in his lab.

References

- [1] J.R. MacCallum, C.A. Vincent, Polymer Electrolyte Reviews-I & II, Elsevier, London, 1987 and 1989.
- [2] a F.M. Gray, Solid Polymer Electrolytes—Fundamentals and Technological Applications, VCH, New York, 1991;

- b F.M. Gray, Polymer Electrolytes, Royal Society of Chemistry Monographs, Cambridge, 1997.
- [3] R.C. Agrawal, G.P. Pandey, J. Phys. D. Appl. Phys. 41 (2008) 223001.
- [4] J.-M. Tarascon, M. Armand, Nature 414 (2001) 359–367.
- [5] M. Watanabe, A. Nishimoto, Solid State Ion. 79 (1995) 306.
- [6] A. Manuel Stephan, K.S. Nahm, Polymer 47 (2006) 5952–5964.
- [7] A. Manuel Stephan, Eur. Polym. J. 42 (2006) 21–42.
- [8] Emad M. Masoud, Alloys Compd. 651 (2015) 157–163.
- [9] Abdelhameed Ahmed ElBellhi, Wafaa Abdallah Bayoumy, Emad Mohamed Masoud, Mahmoud Ahmed Mousa, Bull. Korean Soc. 33 (9) (2012) 2949–2954.
- [10] Emad M. Masoud, A.-A. Elbellhi, W.A. Bayoumy, M.A. Mousa, Alloys Compd. 575 (2013) 223–228.
- [11] E.M. Masoud, A.-A. El-Bellhi, W.A. Bayoumy, M.A. Mousa, Mater. Res. Bull. 48 (3) (2013) 1148–1154.
- [12] Emad M. Masoud, Polym. Test. 56 (2016) 65–73.
- [13] Emad M. Masoud, Mahmoud E. Hassan, Samar E. Wahdaan, Sahar R. Elsayed, Samar A. Elsayed, Polym. Test. 56 (2016) 277–286.
- [14] C. Capiglia, Y. Saito, H. Yamamoto, H. Kageyama, P. Mustarelli, Electrochim. Acta 45 (8–9) (2000) 1341–1345.
- [15] C. Capiglia, Y. Saito, H. Kataoka, T. Kodama, E. Quartarone, P. Mustarelli, Solid State Ionics 131 (3–4) (2000) 291–299.
- [16] D.E. Strauss, D. Golodnitsky, E. Peled, Electrochem. Solid-State Lett. 2 (1999) 115.
- [17] J. Zhou, P.S. Fedkiw, Solid State Ionics 166 (2004) 275.
- [18] G.B. Appetecchi, S. Scaccia, S. Passerini, J. Electrochem. Soc. 147 (2000) 4448.
- [19] M. Moskwiak, I. Giska, R. Borkowska, A. Zalewska, M. Marczewski, H. Marczewska, W. Wieczorek, J. Power Sources 159 (2006) 443.
- [20] L. Sannier, A. Zalewska, W. Wieczorek, M. Marczewski, H. Marczewska, Electrochim. Acta 52 (2007) 5685.
- [21] M. Stolarska, L. Niedzicki, R. Borkowska, A. Zalewska, W. Wieczorek, Electrochim. Acta 53 (2007) 1512.
- [22] V. Aravindan, P. Vickraman, Eur. Polym. J. 43 (2007) 5121–5127.
- [23] D. Saikia, Y.W. Chen-Yang, Y.T. Chen, Y.K. Li, S.I. Lin, Desalination 234 (2008) 24–32.
- [24] A. Manuel Stephen, K.S. Nahm, M.A. Kulandainathan, G. Ravi, J. Wilson, Eur. Polym. J. 42 (2006) 1728–1734.
- [25] R. Kumara, A. Subramania, N.T. Kalyana Sundaram, G. Vijaya Kumarb, I. Baskaran, J. Membr. Sci. 300 (2007) 104–110.
- [26] H.P. Klug, L.E. Alexander, X-ray Diffraction Procedures, Wiley, New York, 1970.
- [27] D. Saikia, A. Kumar, Electrochim. Acta 49 (2004) 2581–2589.
- [28] Z. Li, G. Su, X. Wang, D. Gaw, Solid State Ionics 176 (2005) 1903.
- [29] N.T. Kalyana Sundaram, A. Subramania, Electrochim. Acta 52 (2007) 4987–4993.
- [30] M. Ulaganathan, R. Nithya, S. Rajendran, S. Raghu, Solid State Ionics 218 (2012) 7–12.
- [31] F. Croce, G.B. Appetecchi, L. Persi, B. Scrosati, Nature 394 (1998) 456.
- [32] S.A. Hashmi, H.M. Upahayaya, A.K. Thakur, in: B.V.R. Chodari, W. Wang (Eds.), Solid State Ionics: Materials and Devices, World Scientific, Singapore 2000, p. 461.
- [33] L. Hu, Z. Tang, Z. Zhang, J. Power Sources 166 (2007) 226.
- [34] S. Amderson, J. Am. Ceram. Soc. 38 (1955) 370.
- [35] D. Shanmukaraj, G.X. Wang, R. Murugan, H.K. Liu, Phys. Chem. Solids 69 (2008) 243–248.
- [36] Emad M. Masoud, M. Khairy, M.A. Mousa, Alloys and Compounds 569 (2013) 150–155.
- [37] Emad M. Masoud, Sylvio Indris, RSC Advances 5 (2015) 108058–108066.
- [38] Emad M. Masoud, M.A. Mousa, Ionics 21 (2015) 1095–1103.
- [39] Emad M. Masoud, A.-A. EL-Bellhi, W.A. Bayoumy, Eman M. Same, Ionics 23 (2017) 2417–2427.